

Experimental Freezing of mid-Evolution Fluctuations with a Programmable Annealer

Nicholas Chancellor^{*†&}, Gabriel Aeppli[‡] and Paul A. Warburton[†]

March 26, 2021

†London Centre For Nanotechnology 19 Gordon St, London UK WC1H 0AH

‡Department of Physics, ETH Zürich, CH-8093 Zürich, Switzerland

Department of Physics, École Polytechnique Fédérale de Lausanne (EPFL), CH-1015 Lausanne, Switzerland

Synchrotron and Nanotechnology Department, Paul Scherrer Institute, CH-5232, Villigen, Switzerland

†Department of Electronic and Electrical Engineering, UCL, Torrington Place London UK WC1E 7JE

& Current Affiliation: Department of Physics, Durham University, South Road, Durham, UK

Abstract

For randomly selected couplers and fields, the D-Wave device typically yields a highly Boltzmann like distribution [1] indicating equilibration. These equilibrated data however do not contain much useful information about the dynamics which lead to equilibration. To illuminate the dynamics, special Hamiltonians can be chosen which contain large energy barriers [2, 3]. In this paper we generalize this approach by considering a class of Hamiltonians which map clusters of spin-like qubits (which we will henceforth refer to as 'spins') into 'superspins', thereby creating an energy landscape where local minima are separated by large energy barriers. These large energy barriers allow us to observe signatures of the transverse field frozen. To study these systems, we

assume that these frozen spins are described by the Kibble-Zurek mechanism [4] which was originally developed to describe formation of topological defects in the early universe. It was soon realized that it also has applications in analogous superconductor systems [5, 6, 7, 8] and later realized to also be important for the transverse field Ising model [9, 10]. We demonstrate that these barriers block equilibration and yield a non-trivial distribution of qubit states in a regime where quantum effects are expected to be strong, suggesting that these data should contain signatures of whether the dynamics are fundamentally classical or quantum. We *exhaustively* study a class of 3x3 square lattice superspin Hamiltonians and compare the experimental results with those obtained by exact diagonalisation. We find that the best fit to the data occurs at finite transverse field. We further demonstrate that under the right conditions, the superspins can be relaxed to equilibrium, erasing the signature of the transverse field. These results are interesting for a number of reasons. They suggest a route to detect signatures of quantum mechanics on the device on a statistical level, rather than by observing the behavior for specially chosen Hamiltonians, as was done in [2, 11]. Furthermore, our work suggests that devices of this kind may be able to provide a way of studying the Kibble-Zurek mechanism in large and complex systems, which may be interesting in its own right due to the relevance of Kibble-Zurek to aspects of cosmology as well as condensed matter physics. Finally the Ising square lattice with random fields and couplers is known to be an NP-hard problem [12], meaning that this class of Hamiltonians could provide a potential avenue to

study the effect of dynamical freezing on computation.

1 Introduction

To understand the dynamics of a given system, be it the early universe, or a condensed matter system, it is important to have data which showcase non-equilibrium distributions. Equilibrated data only provide information about the free energy landscape and provide a lower bound on the relaxation rates (the system had to relax fast enough, otherwise one wouldn't see equilibrium). Non-equilibrated data can be understood through the Kibble-Zurek mechanism, in which relaxation rates are assumed to change quickly from an 'adiabatic' regime, where relaxation rates are fast compared to the relevant timescales of the evolution to an 'impulse' regime, where the dynamics are effectively frozen [9]. We call this transition the 'freezing' transition.

The Kibble-Zurek mechanism was first introduced in the context of topological defect formation in the early universe [4]. When a quenched system crosses a phase transition, the relaxation time diverges. During this 'critical slowing down' a transition between the 'adiabatic' and 'impulse' regime can be seen as occurring at a freeze time when the relaxation timescale matches the rate of change of the quench as illustrated in Fig. 1. Any topological defects which are present when this transition occurs will be trapped, even if the system enters the adiabatic regime on the other side of the phase transition [7]. The density of topological defects in the final system is therefore determined by the system at the freeze time, which is in turn related to the rate of the quench. For the annealer there is no re-entry into a new adiabatic regime as there is with defect formation from crossing a phase transition. In this simple case, we approximate the final spin configuration as being the configuration at the freezing point. If freezing happens at a point where quantum fluctuations are still strong, then traces of these fluctuations should be visible at the end of the anneal. As we shall discuss later, we can even define defects on the annealer which behave in an analogous way to the topological

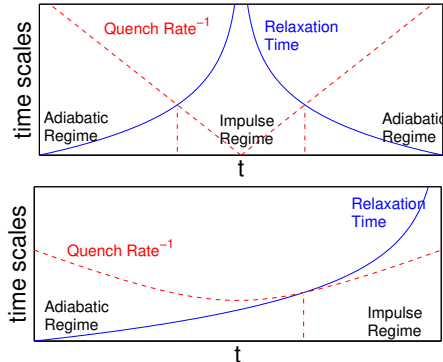


Figure 1: Top, schematic representation of typical Kibble-Zurek mechanism for defect generation: near a phase transition critical slowing down causes the dynamics of a system to be effectively 'frozen'. Crossing this frozen regime leads to topological defects within the system. Bottom, schematic of Kibble-Zurek mechanism for annealer: relaxation time increases as the transverse field is reduced, when this timescale matches the inverse annealing rate, freezing occurs. Frozen in spin configurations can be viewed as "defects" .

defects considered in a more traditional setting for the Kibble-Zurek mechanism.

It is appealing to use this celebrated mechanism to greatly simplify the task of understanding the behavior of a complex system such as the D-Wave device. To this end we consider the simplest possible incarnation of this mechanism. We approximate that under a restricted set of circumstances, to be discussed later, the transition from the 'adiabatic' to 'impulse' regime occurs instantaneously, and always at the same effective temperature and strength of transverse field. While not completely accurate, we will demonstrate that this approximation does capture some important features of the behavior of the device.

The experimental device we use is designed to implement a time dependent transverse Ising model of the following form

$$H(t) = -A(t) \sum_i \sigma_i^x + \alpha B(t) H_{Ising}^{chi} \quad (1)$$

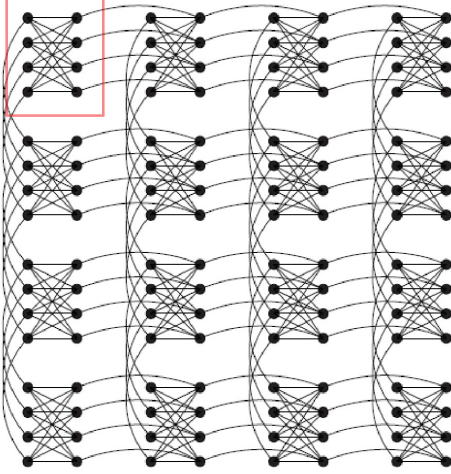


Figure 2: Chimera graphs used for this study. The full figure shows a 4x4 array of unit cells each containing eight spins, a single example of which is shown in the rectangle at the top left of the figure. Each dot represents a spin and each line a coupler.

$$H_{Ising}^{chi} = \left(\sum_i h_i^{chi} \sigma_i^z - \sum_{i,j \in \chi} J_{ij}^{chi} \sigma_i^z \sigma_j^z \right) \quad (2)$$

Here σ^x and σ^z are the Pauli spin matrices, J_{ij}^{chi} and h_i^{chi} are user-programmable local couplers and fields respectively. α sets the overall Ising energy scale. The connectivity of the D-Wave machine is described by the so-called Chimera graph, χ , as shown in Fig. 2. During the course of a single optimization run, $A(t)$ is adiabatically reduced to near zero in a manner analogous to simulated annealing in which the scale of thermal fluctuations (*i.e.* the temperature) is reduced to zero. At $t = t_f$ the system is described by $H(t) \approx \alpha B(t) H_{Ising}^{chi}$ and the dynamics are fully classical. Unfortunately, the rates at which $A(t)$ and $B(t)$ can be changed experimentally is limited, and therefore a 'typical' case of randomly selected fields and couplers for H_{Ising}^{chi} will yield an equilibrium result, even at the fastest allowed sweep rate [1].

It has already been demonstrated however [2] that flipping a fully connected chimera unit cell creates

an energy barrier which is high enough to prevent equilibration. Based on this observation, we replace H_{Ising}^{chi} in Eq. 2 by a restricted set of 'superspin' Hamiltonians H_{Ising}^{ss} :

$$H(t) = -A(t) \sum_i \sigma_i^x + \alpha B(t) H_{Ising}^{ss}. \quad (3)$$

Here all couplers within a unit cell are of maximum allowed strength and ferromagnetic

$$H_{Ising}^{ss} = - \sum_{i,j \in \chi_{int}} \sigma_i^z \sigma_j^z + \alpha_s H_{ss}, \quad (4)$$

and

$$H_{ss} = \left(\sum_i \frac{1}{2} \sigma_i^z - \sum_{i,j \in \chi_{ext}} J_{ij} \sigma_i^z \sigma_j^z \right). \quad (5)$$

In this case we divide the graph $\chi \equiv \chi_{int} \cup \chi_{ext}$, where χ_{int} indicate the couplers within a unit cell and χ_{ext} the couplers between unit cells. $\alpha_s \cdot \alpha$ sets the overall energy scale of the superspin Hamiltonian. Hamiltonians of this type will have an energy landscape in which every state for which all of the spins within a unit cell agree is a local minimum. We can therefore think of the low energy dynamics of this Hamiltonian as that of an effective Hamiltonian in which each unit cell behaves like a single spin. The underlying graph of these superspin Hamiltonians is a square lattice, as demonstrated in Fig. 3.

If the entire chimera graph is used in this way, then the overall field for each superspin is $h_s = 4\alpha \cdot \alpha_s$ while the energy of each of the couplers is $J_s = \pm 4\alpha \cdot \alpha_s$. On the other hand if we consider truncated chimera unit cells consisting of only 4 spins the fields and couplers take values $h_s = 2\alpha \cdot \alpha_s$, while the energy of each of the couplers is $J_s = \pm 2\alpha \cdot \alpha_s$. We choose $|h_s| = |J_s|$ so that the effective superspin Hamiltonian is reminiscent of the Hamiltonian used in [1]. As was the case for the single chimera unit cell in [1], we can simplify our task by examining only symmetry inequivalent Hamiltonians. For the 3x3 square lattice this use of symmetry equivalent reduces the number of Hamiltonians we must investigate from 2^{12} to a more manageable 570. Because of the local gauge

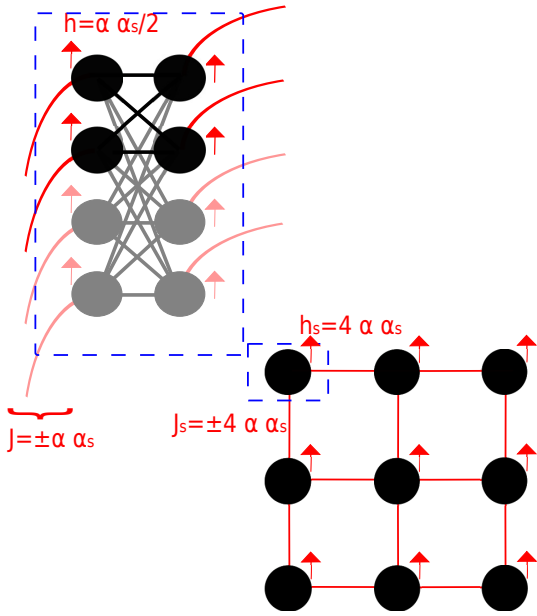


Figure 3: Mapping of an effective square lattice Hamiltonian onto the chimera graph using superspins. Runs with the truncated unit cell utilize only the full colour part of the cell, while runs with the whole cell include the faded part. All internal couplers are ferromagnetic and of strength α .

symmetry, this is also the set of symmetry inequivalent Hamiltonians for the larger (2^{21}) set in which $h_s \propto \pm \alpha \cdot \alpha_s$.

Experimental methods

All experiments were performed on the D-Wave Vesuvius processor located at the Information Sciences Institute of the University of Southern California. This processor contains 512 bits in an 8×8 array of unit cells. Due to fabrication errors, nine of the bits fall outside of the acceptable calibration range. We elected to study a 3×3 patch of unit cells which did not contain any of these defective bits. The annealing time t_f was fixed at $20 \mu s$ except where otherwise stated. All data were sampled over randomized gauges and transformations under the dihedral symmetry of the square lattice.

2 Calculation Method: spin-sign transitions

Motivated by the relationship to real world inference problems [1] and the fact that we desire to look at discrete rather than continuous problems, we chose to restrict our analysis to examining the sign of mean spin orientations. Examining the sign only rather than the full mean orientation simplifies our analysis greatly, as knowledge of the locations where the mean orientation of the spins pass through zero plus the sign of the orientation at high temperature allow complete knowledge of the sign of the orientation for the entire parameter space. We refer to these zeros as *spin-sign transitions*.

Each spin within a Hamiltonian will have a finite (possibly empty) set of spin-sign transitions with temperature. This concept can be easily extended to include transverse field, with spin sign-transitions as 1 dimensional curves in $T-\Delta$ space, rather than points. In one dimension the spin-sign transitions are the nodes of a function, in 2D the nodes become 1 dimensional lines. For the effective superspin Hamiltonian shown in Fig. 3, these transitions can be readily calculated using exact diagonalization. These spin-sign transitions (along with the sign of the orienta-

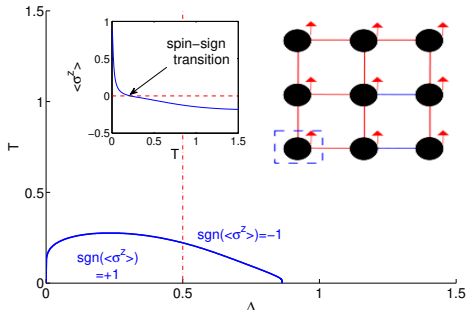


Figure 4: An example of a spin-sign transition, which divides regions of phase space where $\text{sgn}(\langle \sigma^z \rangle) = +1$ and $\text{sgn}(\langle \sigma^z \rangle) = -1$ calculated using exact diagonalization. The transition occurs when the mean orientation of the spin in the lower left corner of the 3×3 Hamiltonian shown in the inset changes sign. All fields and couplings have the same magnitude, with red indicating anti-ferromagnetic coupling and blue indicating ferromagnetic. The inset plot shows the polarization versus temperature on the $\Delta = 0.5$ line and the associated spin-sign transition.

tion somewhere not directly on a transition) allow us to know the sign of the orientation of every spin for any value of temperature and transverse field. Fig. 4 shows an example of a single spin-sign transition, appearing as a line which divides regions of phase space where $\text{sgn}(\langle \sigma^z \rangle) = +1$ and $\text{sgn}(\langle \sigma^z \rangle) = -1$.

We have two complementary goals for our spin-sign transition analysis, firstly we want to be able to define defects for the Kibble-Zurek mechanism to act upon and estimate the 'freeze time' when the dynamics become slow enough that the system can be viewed as 'frozen'. We define a *spin-sign defect* as a spin for which the orientation has a different sign than the one predicted for the final (finite temperature) configuration at the end of the anneal. If the system remained perfectly adiabatic throughout the evolution, then there would be no spin-sign defects, analogous to topological defects in a more traditional setting for the Kibble-Zurek mechanism. This analysis assume simple monotonic behavior of the defect density, and therefore is most appropriate for spins

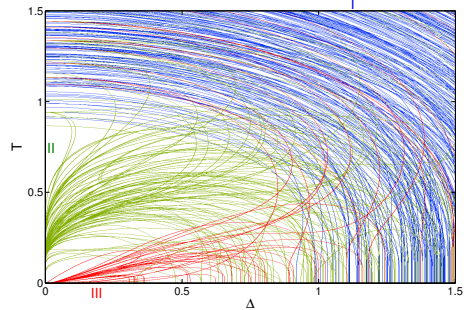


Figure 5: Spin-sign transitions for a 3×3 transverse field Ising square lattice, exhaustively calculated for all 570 symmetry inequivalent Hamiltonians. Colours indicate whether transitions are associated with type I II or III spins.

whose spin-sign transitions form simple arc like paths in T - Δ space, as the transitions labeled I in Fig. 5 do. We term this type of analysis 'defect rate analysis'.

On the other hand, we want to be able to compare our experimental results to static exact diagonalization calculations at a range of temperature and transverse field values and be able to detect signatures of the conditions when the system froze. One concern, especially in light of the analysis performed in [13, 14] is that there will be little difference between the effect of finite temperature and finite transverse field, and spin-sign transitions will not provide a reliable way of distinguishing between thermal and transverse field effects. Fig. 5 demonstrates that the spins labeled II and III have complex structures in their spin-sign transitions which will allow us to distinguish these two effects. We term this type of analysis 'frozen spin analysis'.

Many of the spin-sign transitions however do form arc-like paths in T - Δ space consistent with the results from [13, 14] and that for higher T and Δ these transitions dominate completely, see Sec. 1 of the supplemental material.

Before going further, we need to discuss the method which we have employed in classifying these spins. We first note that the highly non-arc-like spin-sign transitions tend to cross through the ori-

gin point, $(T, \Delta = 0)$. It is therefore interesting to consider these spins separately from those which do not have a transition which crosses the origin. A spin will have a spin-sign transition at the origin if it does not have a definite *ground state orientation*; in other words, spins for which there are an equal number of states with spin up as down in the zero transverse field ground state manifold. However, this is not the only way in which that feature can come about. If the point $T, \Delta = 0$ is approached classically, i.e. by reducing temperature at zero transverse field, the orientation will agree with the ground state orientation. On the other hand approaching this point quantum mechanically, by reducing transverse field at zero temperature, holds no such guarantee. The ground state orientation at infinitesimal transverse field therefore need not have the same sign of an unweighted sampling of the classical ground state manifold, leading to a spin sign transition at zero temperature and infinitesimal Δ . We therefore divide the spins into 4 types:

Type 0 No spin-sign transitions, the sign of the orientation does not change at any value of T or Δ . These spins are of no interest to this study. Of all 5130 spins considered 3835 have no spin-sign transitions between $0 \leq T < 5$ and $0 \leq \Delta < 5$, and therefore can be considered to be type 0 for our purposes.

Type I Spin-sign transitions present, but no spin-sign transition at $T, \Delta = 0$. These transitions form arc-like paths far from the origin, consistent with the behaviour seen in [13, 14]. We found 844 spins for which there were spin-sign transitions in the range $0 \leq T < 5$ and $0 \leq \Delta < 5$ but which did not have a transition at $T, \Delta = 0$. These are the spins of interests for defect rate analysis.

Type II No definite ground state orientation, there are an equal number of states with the spin up and spin down in the zero transverse field ground state manifold, by construction these have a spin-sign transition at $(T, \Delta = 0)$. We observe that 411 of the spins are type II. From Fig. 5 we can see that these spins possess a complex spin-

sign transition structure which is not desirable for defect rate analysis, but is highly desirable in frozen spin analysis.

Type III Definite ground state orientation, but quantum fluctuations from an infinitesimal Δ stabilize an orientation with the opposite sign. We observe that 40 of the spins are type III. From Fig. 5 we can see that these spins also possess a complex spin-sign transition structure which is not desirable for defect rate analysis, but is highly desirable in frozen spin analysis.

There is no restriction the spin-sign transitions for a single need to form a connected graph, therefore spins of type II and III may still also have arc-like transitions far from the origin.

For the defect rate analysis we only want to count defects for type I spins. For the frozen spin analysis on the other hand, we compare the sign of the experimentally observed orientation of all type I, II and III superspins to the theoretical equilibrium value from the effective superspin Hamiltonian at different values of temperature and transverse field. The spin orientations of these Hamiltonians can be readily calculated by exact diagonalization. It is worth emphasizing that this is a completely static quantity, and while there is theoretical justification for comparing this quantity to our experimental data, such comparison represents a gross simplification.

A highly simplified version of Kibble-Zurek where all Hamiltonians with the same α and α_s all transition instantly from the 'adiabatic' to the 'impulse' regime, (i.e. freeze) at the same point in the annealing process predicts perfect agreement at some value of T and Δ . It is in this sense that the frozen spin analysis assumes a very simple version of Kibble-Zurek. In Sec. 4 we will show data which suggests that, while not completely accurate, this highly simplified picture does allow us to obtain non-trivial signatures of the behavior of the spins at the point when they freeze. However before this we perform a more traditional Kibble-Zurek analysis in Sec. 3.

3 Rate of Spin-Sign defects

Before we compare in detail the spin orientations at every point in T - Δ space, it is worth considering a defect density calculation in analogy to what is usually considered for a condensed matter or cosmological system undergoing the Kibble-Zurek mechanism. To do this we must define a defect. We define a spin-sign defect as a spin for which the orientation has a different sign than the one predicted for the final (finite temperature) configuration at the end of the anneal. If the system remained perfectly adiabatic throughout the evolution, then there would be no spin-sign defects, analogous to topological defects in a more traditional setting for the Kibble-Zurek mechanism.

One complication with defining spin-sign defects in such a way is that these defects will not necessarily decrease monotonically in number throughout the annealing process. Fortunately, we observe that type I spins have highly arc-like spin-sign transitions, and therefore should show a monotonic decrease in equilibrium defect number during the annealing protocol, Fig. 6 shows that this is indeed the case. The number of defects on type I spins decreases with increasing annealing time, consistent with the Kibble-Zurek mechanism, and suggests an effective 'freeze time' for (at least a subset of) type I spins around $t/t_f = 0.5$ which becomes slightly later as t_f is increased. Given the low rate of defects, another possible interpretation is that freezing actually occurs at $t/t_f \gg 0.5$, and the defects seen here are anomalies which are not captured in our simplified Kibble-Zurek picture. To answer determine which interpretation is correct, we must perform a numerical estimate of the freeze time.

To perform a numerical estimate of the freeze time we ideally would like to exactly diagonalize the 3×3 truncated chimera graph and use open quantum system techniques to estimate the decay rate. Unfortunately, the number of spins is outside of the range which we can numerically access with standard ED techniques. To accurately describe the freezing process however we want to go beyond the simple spin $\frac{1}{2}$ description of the superspins used elsewhere in this manuscript.

To capture the internal freezing behavior of the

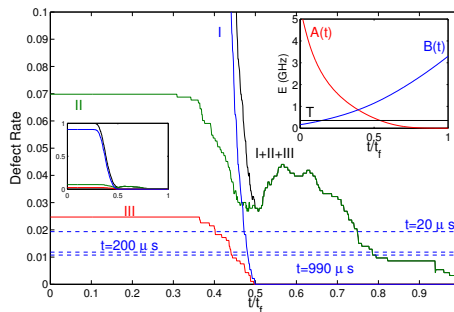


Figure 6: Equilibrium defect rate for different spin types in the effective (9 spin) superspin Hamiltonian for $\alpha = 0.25$, $\alpha_s = 1$ with a truncated 4-spin unit cell versus t/t_f . A rate of 1 corresponds to defects on 931 of the spins. Dotted lines are the number of defects in type I spins observed in experimental runs over $20\mu s$, $200\mu s$, and $990\mu s$. The number of defects decreases with slower anneal time, as predicted by the Kibble-Zurek mechanism. The black line represents all defects, while the blue represents type I only, the gold type II and the red type III. Left inset: full range of y axis. Right inset: annealing schedule.

superspines, while still operating in a numerically tractable regime, we approximate each truncated chimera unit cells as a $K(4)$ fully connected graph in which each spin couples equally to the all of the spins in adjacent superspins. We take the internal coupling strength to be the average couplings between the spins in the chimera. This approximation endows each unit cell with full permutation symmetry, meaning that as long as the symmetry is unbroken each can be described by 5 states. This is in contrast to the actual $K(2, 2)$ graph of the truncated chimera unit cell, for which 9 states are required.

To estimate the freeze time we choose to focus on the Hamiltonian for which all couplings are ferromagnetic, this allows us to further reduce the size of the computation by taking advantage of the fact that this choice of Hamiltonian does not break the dihedral symmetry of the 3x3 square graph. For the relaxation timescale we calculate the decay rate from the first excited state to the ground state using standard Redfield formalism with realistic coupling parameters [18, 19] assuming a dominant coupling to the bath in the σ^z direction.

We approximate the quench rate as the magnitude of the overlap between the ground and first excited state at times which are separated by an infinitesimal time step Δt divided by Δt ,

$$\frac{|\langle \psi_0(t) | \psi_1(t + \Delta t) \rangle|}{\Delta t}. \quad (6)$$

The numerical data in Fig. 7 suggest that the freeze time for $t_f = 20\mu s$ is indeed around $t/t_f = 0.5$, and therefore the larger number of defects seen for this anneal time (compared with $t_f = 200\mu s$ and $t_f = 990\mu s$) can be explained by the Kibble-Zurek mechanism assuming all Hamiltonians freeze at the same time. On the other hand, for $t_f = 200\mu s$ and $t_f = 990\mu s$, the freeze time is predicted to be much later, indicating that the type I defects seen in these cases are anomalies which are not well described by one or more of the approximations we apply.

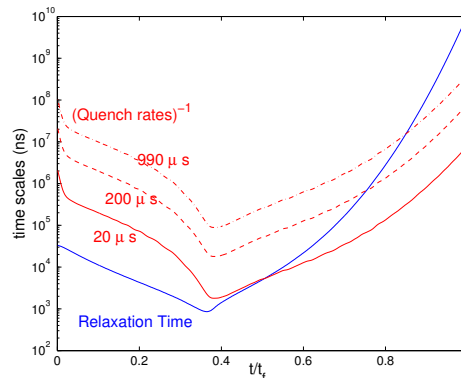


Figure 7: Comparison of inverse quench rates approximated by $\frac{|\langle \psi_0(t) | \psi_1(t + \Delta t) \rangle|}{\Delta t}$ where $\Delta t = t_f/1000$ for the 3 annealing times examined in Fig. 6 versus relaxation time induced by the bath. This plot is based on an approximation where chimera unit cells are treated as fully connected graphs. The Kibble-Zurek approximation is to assume that the system freezes when the inverse quench rate becomes equal to the relaxation time.

4 Frozen in Behavior of Spins

Comparison between the experimental data and the static exact diagonalization model appear in Figs. 8 and 9. In these figures, the experimentally observed sign of the spin orientations are compared with the static superspin model at various values of temperature and transverse field. In subfigures b)-d) of these figures the number of disagreements with the exact diagonalization model is represented as a fraction of the 1295 spins for which we observed a spin-sign transition in the superspin model for $0 \leq T < 5$ and $0 \leq \Delta < 5$. It is worth noting that we do not consider the 3835 remaining (type 0) spins for which there is no transition, as the sign of the orientation of these spins contains no useful information as to the values of temperature and transverse field which the device has experienced. Subfigure a) of these two figures plots the region where the disagreement for the remaining subfigure is close to minimal, and therefore facilitates direct comparison between the data in the

other subfigures.

Fig. 8 demonstrates that for $\alpha = 1$ the data agree best with the behavior at low temperatures and moderate transverse field. Moreover, as α_s is reduced, the transverse field for best agreement increases. This trend is what we should expect in a Kibble-Zurek mechanism picture, where the energy scale of the couplers in the superspin Hamiltonian α_s is reduced relative to the transverse field. This indicates that our approach is successful, on average, at trapping remnants of the transverse fields, and that we have successfully captured data outside of the Boltzmann like equilibrium expected at $t = t_f$. It is encouraging that the best agreement is in a regime where transverse field is similar in strength to the couplers, and temperature is low, as this is the regime where quantum fluctuations are expected to be the strongest. While suggestive, this fact in itself is not conclusive evidence of quantum behavior, as there may be mean field models of the form [15, 16] which also behave in this way. Showing that we can access this regime however is an interesting result in itself, as it suggests that further analysis of this data will likely prove fruitful for examining the role which quantum effects play.¹ Compared to the quantum calculation, the classical spin calculation is much more numerically intensive, and we are currently working on analysis in this direction.

These data are also interesting in that they show that a much simplified Kibble-Zurek description of the device allows us to detect traces of the dynamics in a non-trivial way. Unsurprisingly, however there is no value of T and Δ for which the data agree perfectly with static conditions of finite temperature and transverse field. This is to be expected given the large number of approximations which must be made to assume that the chip data would agree perfectly. Here we list some possible reasons for imperfect agreement: the internal degrees of freedom of the superspins (the individual spins) may lead to non-trivial corrections; not all Hamiltonians may freeze at the same time; the superspins themselves may not freeze uniformly for a

¹Authors Note: We are currently in the process of obtaining access to computing resources so that we can perform classical simulations for comparison, results to appear in subsequent pre-prints and published version.

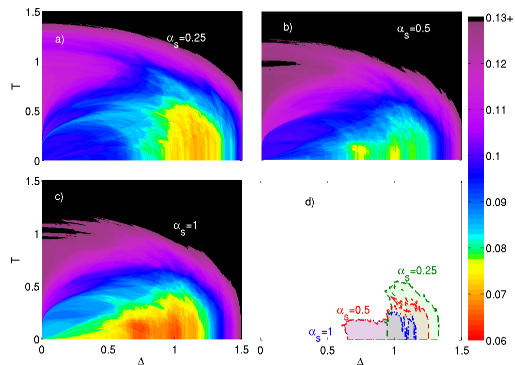


Figure 8: a-c) Colour plots indicating the fraction of bits which disagree with finite temperature and transverse field states for the effective superspin Hamiltonian for $\alpha = 1$ and different values of α_s as follows a) $\alpha_s = 0.25$ b) $\alpha_s = 0.5$ c) $\alpha_s = 1$. Δ and T are both in dimensionless units. d) lines and shading indicate parameter regimes where the number of disagreements is 10 or less away from the best agreement. All data in this plot are for an anneal time of $20 \mu s$. Note that bits with no spin-sign transition were excluded from these plots. Δ and T are both in dimensionless units.

given Hamiltonian; control errors may cause order-by-disorder effects which do not average out and/or; Interaction with the bath may change the Hamiltonian spectrum via the Lamb shift [17].

To demonstrate that this effect is in fact Kibble-Zurek, we examine the effect of longer annealing times. In Fig. 9, the data tend to agree more strongly with model with lower transverse field as this time is increased. This is consistent with the data having time to equilibrate during the longer anneals, and traces of the transverse field being erased.

Note that Fig. 9 shows data with a truncated 4 spin unit cell and $\alpha = 0.25$, $\alpha_s = 1$, rather than the full 8 spins. For the full 8 spin system, even at low values of α , equilibration could be observed for anneal times up to $2000 \mu s$ (see Sec. 2 of the supplemental material). We suspect that the reason for this is that we are unable to experimentally access the timescales which are required to reach equilibrium. This is reasonable, because for an isolated su-

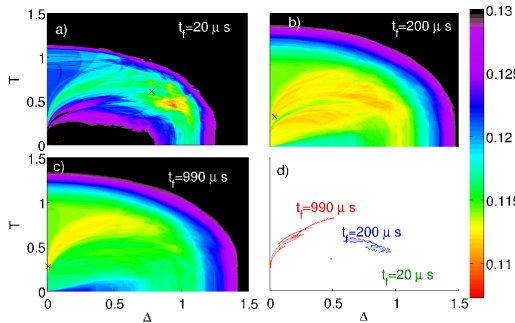


Figure 9: Plots of truncated cell with two spins on each side $\alpha = 0.25$, $\alpha_s = 1$ run for various anneal times. a-c) Colour plots indicating the fraction of bits with spin sign transitions which disagree with finite temperature and transverse field states for the effective superspin Hamiltonian as follows b) $t = 20 \mu s$ c) $t = 200 \mu s$ d) $t = 990 \mu s$. d) lines and shading indicate parameter regimes where the number of disagreements is 3 or less away from the best agreement. Δ and T are both in dimensionless units. X indicates freezing parameters from Fig. 7.

perspin (without fields) based on the full unit cell flipping the superspin only comes in at fourth order of perturbation theory and has an effective potential barrier of $16 \alpha B(t)$. Flipping the truncated version of the other hand only requires second order in perturbation theory and comes with an energy barrier of only $4 \alpha B(t)$.

5 Conclusions

We have demonstrated that we are able to detect remnants of the dynamics in a non-trivial way by using a class of superspin Hamiltonians which feature strong energy barriers. These data suggest that we are able to preserve information from a regime of low temperature and moderate transverse field, which is exactly the regime where quantum behaviors are expected to be the strongest. With further numerical classical spin calculations, one should be able to distinguish between classical and quantum behavior. Moreover the observation of this mechanism on the

D-Wave device suggest that the device may be useful in studying the Kibble-Zurek mechanism in highly complex Ising systems, an interesting prospect in its own right, given the the importance of this mechanism to aspects of cosmology and condensed matter physics. These experiments are also tantalizing because the underlying superspin Hamiltonians map to a class of NP-hard problems [12], and therefore may also be interesting in illuminating the effect which the Kibble-Zurek mechanism may have on computation.

Acknowledgements

This work was supported by Lockheed Martin and by EPSRC (grant refs: EP/K004506/1 and EP/H005544/1). We thank the USC Lockheed Martin Quantum Computing Center at the University of Southern California’s Information Sciences Institute for access to their D-Wave Two machine. We acknowledge fruitful discussions with Andrew Green, Szilard Szoke, and Markus Mueller and thank Mohammad Amin for providing the Redfield code on which we based our relaxation time calculation.

References

- [1] Chancellor, N. Szoke, S. Vinci, W. Aeppli, G. and Warburton, P. A. Maximum-Entropy Inference with a Programmable Annealer Scientific Reports 6, 22318 (2016).
- [2] S. Boixo et al. *Computational Role of Multiqubit Tunneling in a Quantum Annealer* arXiv:1502.05754 (2015)
- [3] S. Boixo, T. Albash, F. M. Spaldalieri, N. Chancellor, D. A. Lidar, *Experimental signature of programmable quantum annealing* Nature Comm. 4, 3067 (2013).
- [4] T. W. B. Kibble *Topology of Cosmic Domains and Strings* J. Phys. A : Math. Gen., Vol. 9, No. 8. (1976)
- [5] W. H. Zurek *Cosmological Experiments in Superfluid Helium?* Nature Vol. 317 (1985)

- [6] T. W. B. Kibble *Cosmology in the Laboratory* Nature Vol. 317 (1985)
- [7] W. H. Zurek *Cosmological Experiments in Condensed Matter Systems* Physics Reports 276 177-221(1996)
- [8] W.H Zurek *Cosmic Strings in Laboratory superfluids and the Topological Remnants of Other Phase Transitions* Acta Physica Polonica Vol. 24 No. 7 (1993)
- [9] B. Damski *The Simplest Quantum Model Supporting the Kibble-Zurek Mechanism of Topological Defect Production: Landau-Zener Transitions from a New Perspective* PRL 95, 035701 (2005)
- [10] J. Dziarmaga *Dynamics of a Quantum Phase Transition: Exact Solution of the Quantum Ising Model* PRL 95, 245701 (2005) .
- [11] T. Lanting et. al. *Entanglement in a Quantum Annealing Processor* Phys. Rev. X 4, 021041 (2014)
- [12] F. Barahona, *ON THE COMPUTATIONAL-COMPLEXITY OF ISING SPIN-GLASS MODELS* Journal of Physics a-Mathematical and General 15 3241 (1982).
- [13] Y. Otsubo et al. *Effect of quantum fluctuation in error-correcting codes* Phys. Rev. E 86 051138 (2012).
- [14] Y. Otsubo et al. *Code-division multiple-access multiuser demodulator by using quantum fluctuations* Phys. Rev. E 90, 012126.
- [15] P. J. D. Crowley and A. G. Green *An Anisotropic Landau-Lifschitz-Gilbert model of dissipation in qubits* arXiv:1503.00651 (2015)
- [16] S. Shin et al. "Comment on *Distinguishing Classical and Quantum Models for the D-Wave Device* arXiv:1404.6499 (2014).
- [17] T. Albash, S. Boixo, D. A. Lidar, and P. Zanardi *Quantum Adiabatic Markovian Master Equations* New J. Phys. 14 123016 (2012)

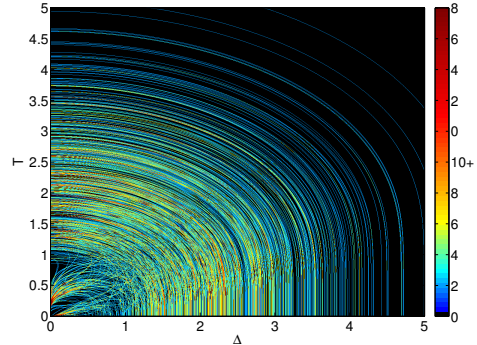


Figure S1: Density of spin sign transitions for a wider range of T and Δ then Fig. 3 of the main text.

[18] We are grateful to Mohammad Amin for providing us numerical code on which we based this calculation.

[19] H. -P. Breuer and F. Petruccione *the Theory of open Quantum Systems* Oxford University Press 2002.

Supplemental Material for: Experimental Freezing of mid-Evolution Fluctuations with a Programmable Annealer

6 Spin-sign transitions at higher temperature and transverse field

Fig. 3 of the main manuscript illustrates the spin-sign transitions for $0 < T < 1.5$ and $0 < \Delta < 1.5$. Fig. S1 illustrates that at higher values of T and Δ , the transition densities follow arcs. This is consistent with the results found in [13, 14], which predict little difference between the ability to decode using thermal fluctuations and quantum fluctuations.

Based on the shape of these transitions, we are not able to reliably distinguish between the effects of temperature and transverse field, as Fig. S2 demonstrates.

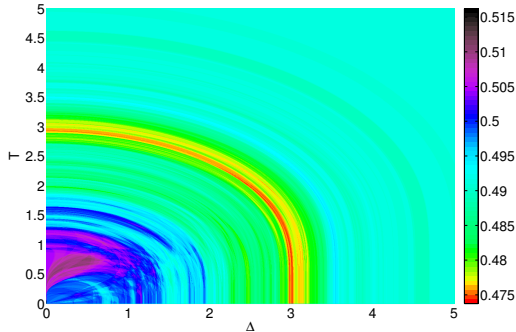


Figure S2: Colour plots indicating the fraction of bits with spin-sign transitions which disagree with finite temperature and transverse field states for the effective superspin Hamiltonian for $\alpha = 1$ and $\alpha_s = 0.1$.

7 Full unit cell with $2000\mu s$ annealing time

While we are able to demonstrate equilibration with a truncated unit cell as illustrated in Fig. 5 of the main document, we were not able to see the same kind of behavior for superspins based on the full chimera unit cell. Fig. S3 illustrates that even if the energy scale α is reduced to 0.15 and the annealing time increased to $2000\mu s$, the data still show remnants of the transverse field.

References

- [1] Y. Otsubo et al. *Effect of quantum fluctuation in error-correcting codes* Phys. Rev. E 86 051138 (2012).
- [2] Y. Otsubo et al. *Code-division multiple-access multiuser demodulator by using quantum fluctuations* Phys. Rev. E 90, 012126.

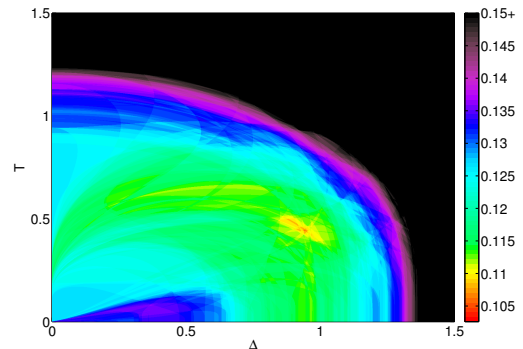


Figure S2: Colour plots indicating the fraction of bits with spin sign transitions which disagree with finite temperature and transverse field states for the effective superspin Hamiltonian for $\alpha = 0.15$, $\alpha_s = 1$ and a run time of $2000\mu s$.